The final publication is available at

http://doi.org/10.1021/acschemneuro.1c00758

Additional Information

Neuroprotective effect of IND1316, an indole-based AMPK activator, in animal models of Huntington disease

Marta Vela,[†,#] M Adelaida García-Gimeno,[‡,#] Ana Sanchis,[§#] José Bono-Yagüe,[§] José Cumella,[†] Laura Lagartera, [†] Concepción Pérez, [†] Eva Mª Priego,[†] Angela Campos,[$] Pascual Sanz,[$,*] Rafael P. Vázquez-Manrique, [&,*] Ana Castro[†,*]

[†] Instituto de Química Médica, IQM-CSIC, Juan de la Cierva 3, 28006-Madrid, Spain.

[‡] Department of Biotechnology, Escuela Técnica Superior de Ingeniería Agronómica y del Medio Natural (ETSIAMN), Universitat Politécnica de València, 46022-Valencia, Spain.

[§] Grupo de Investigación en Biomedicina Molecular, Celular y Genómica, Instituto de Investigación Sanitaria La Fe (IIS La Fe), 46026-Valencia, Spain and Joint Unit for Rare Diseases IIS La Fe-CIPF, 46012-Valencia, Spain

[&] Grupo de Investigación en Biomedicina Molecular, Celular y Genómica, Instituto de Investigación Sanitaria La Fe (IIS La Fe), 46026-Valencia, Spain; Joint Unit for Rare Diseases IIS La Fe-CIPF, 46012-Valencia, Spain and Centro de Investigación Biomédica en Red de Enfermedades Raras (CIBERER)-ISCIII, 28029-Madrid, Spain.

[$] Instituto de Biomedicina de Valencia, IBV-CSIC, 46010-Valencia, Spain and Centro de Investigación Biomédica en Red de Enfermedades Raras (CIBERER)-ISCIII, 28029-Madrid, Spain.

# These authors contributed equally to this work.
* These three Co-corresponding authors contributed equally to this work.

ABSTRACT

Aggregation of mutant huntingtin, due to an expanded polyglutamine track, underlies the cause of neurodegeneration in Huntington disease (HD). However, it remains unclear how some alterations at the cellular level lead to specific structural changes in HD brains. In this context, the neuroprotective effect of the activation of AMP-activated protein kinase (AMPK) appears to be a determinant factor in several neurodegenerative diseases, including HD. In the present work, we describe a series of indole-derived compounds able to activate AMPK at the cellular level. By using animal models of HD (both worms and mice), we demonstrate the *in vivo* efficacy of one of these compounds (IND1316), confirming that it can reduce neuropathological symptoms of this disease. Taken together, *in vivo* results and *in silico* studies of druggability, allow us to suggest that IND1316 could be considered as a promising new lead compound for the treatment of HD and other central nervous system diseases in which activation of AMPK results in neuroprotection.

KEYWORDS: indole derivatives, AMPK, neuroprotection, ADME *in silico*, *C. elegans* models, polyQ toxicity, Huntington disease mouse models.

INTRODUCTION

Huntington disease (HD) is a progressive, autosomal dominant neurodegenerative disorder that causes alterations in motor coordination together with symptoms characterized by involuntary movements, cognitive impairment, and mental deterioration. The disease is caused by an abnormally long expansion of trinucleotide CAG in the *HTT* gene, leading to the production of a cytosolic protein, of yet unclear function,[1] called huntingtin (Htt). Carriers of an expansion of 36 or more CAG trinucleotides express a mutant version of Htt (mHtt), which contains a tandem of glutamines (polyQ) that makes the protein unstable and prone to aggregation. The process of aggregation produces toxic species of mHtt, both soluble and in form of aggregates,[2,3] that disrupt key cellular processes (e.g. autophagic flow, axonal transport, transcription of some genes, synaptic function, etc.) which in turn induces neuronal degeneration.

AMP-activated protein kinase (AMPK) acts as a key player in regulating energy metabolism. This enzyme is a heterotrimer (AMPKα is the catalytic and AMPKβ and AMPKγ are regulatory subunits) that is activated when there is a drop in the levels of ATP. Activation of AMPK inhibits anabolic pathways and activates catabolic pathways to restore energy levels. AMPK plays a very important role in brain physiology as a metabolic sensor of the central nervous system, ensuring the maintenance of energy homeostasis. [4] In particular, it has been described that drugs that activate AMPK lead to a neuroprotective effect in several neurodegenerative diseases.[4,5,6] The most representative example is metformin, which has demonstrated its therapeutic potential for the treatment of Alzheimer's disease,[7] Parkinson's disease,[8] and HD. [9,10]

Related to the role of AMPK as a therapeutic target in HD, several groups have reported that AMPK activation prevents the toxic effects induced by mHtt species,

based on both invertebrate models of polyQ toxicity (*C. elegans*) [10,11,12] and mouse

models of HD.[9,10] These results, together with the improvement in cognitive function

after metformin administration in HD patients, who also have type 2 diabetes,[13] indicate

that the pharmacological activation of AMPK might be a potential strategy to address

HD. To reinforce this hypothesis and following with our AMPK drug discovery

programs,[14] we performed a screening of our in-house chemical library. As result, we

report herein the therapeutic potential of new AMPK activators as neuroprotective

agents by describing the synthesis, the *in silico* ADME properties prediction, and

AMPK activation studies of three new aryl indole derivatives (Figure 1). In addition,

one of these compounds, IND1316, has been evaluated for its neuroprotective activity
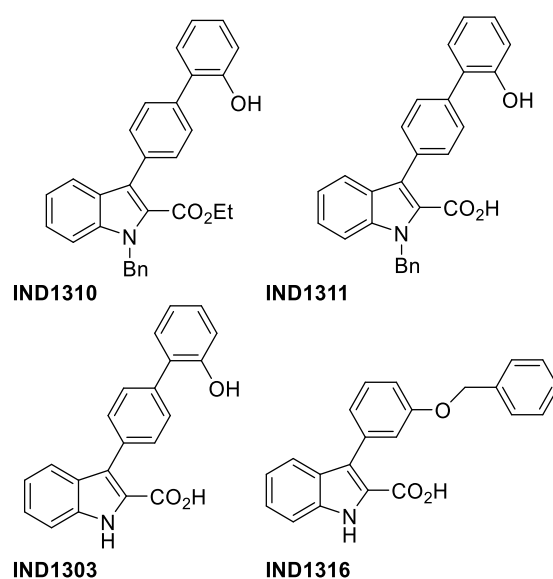
in animal models of HD.

Figure 1: Chemical structure of the indole compounds analyzed in this work.

RESULTS

Chemistry

IND1303, IND1310, IND1311, and IND1316 (Figure 1) were synthesized following the

synthetic route outlined in Scheme 1 in which iodization of compound 2 was obtained

according to the procedure previously described.[14] Benzyl derivative 3 was prepared by an alkylation reaction of compound 2 with benzyl bromide under standard benzylation conditions. Finally, target compounds were prepared following a two-step protocol based on a C-C coupling reaction with the appropriated boronic acid and basic deprotection using KOH.
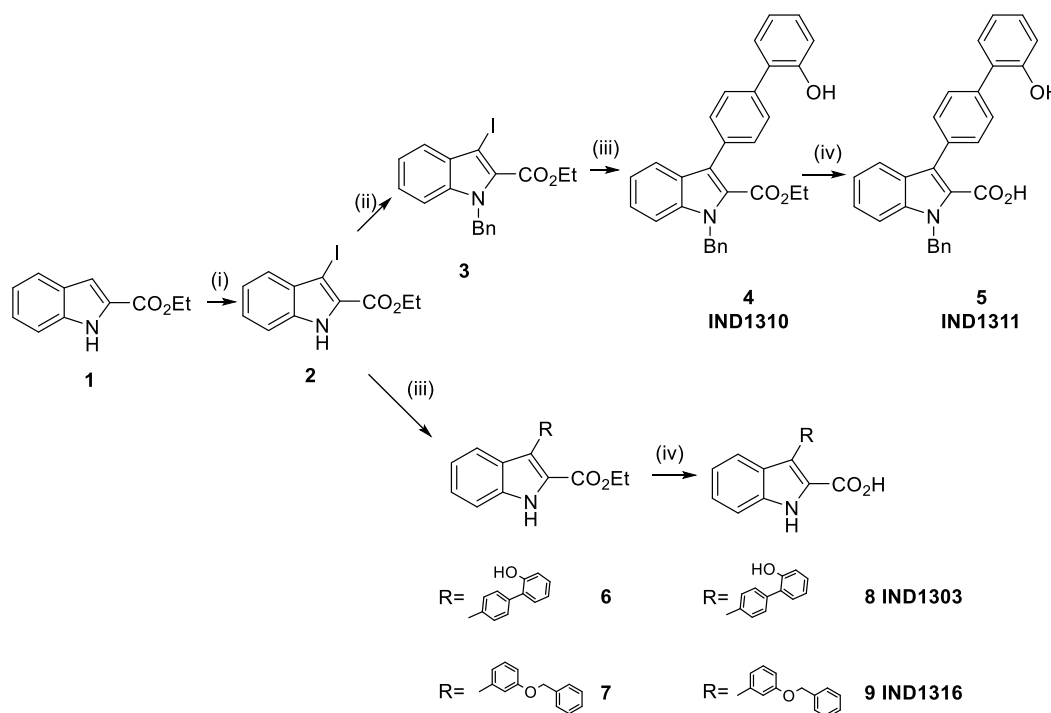
Scheme 1: (i) N-iodosuccinimide, DMF, 0°C, 1 h; (ii) NaH, DMF, BrBn, r.t., 2 h; (iii) Dioxane:toluene:ethanol:water (10:1:3:6), R-B(OH)$_2$, Pd(dppf)Cl$_2$, K$_2$CO$_3$, 85°C, 2-18 h; (iv) EtOH:H$_2$O (2:1), KOH, 100°C, 3 h.

AMPK activity in HEK293 cells, structure-activity relationship (SAR), and toxicity studies

To determine the ability of the indole derivatives 4, 5, 8, and 9 to regulate AMPK activity at the cellular level, AMPK activation assays in HEK293 cell lines were carried out with target compounds (see Materials and Methods). Cells treated with 5 mM phenformin were used as a positive control of AMPK activation. We observed that

compounds IND1303, IND1311, and IND1316 produced a dose-dependent increase in Thr172 phosphorylation of AMPKα compared to untreated control cells, an indication of AMPK activation (levels of AMPKβ1 were used as a loading control) (Figure 2). The efficiency in activating AMPK varied among the compounds, being IND1316 the product that activated AMPK at a much lower concentration. Moreover, to demonstrate the functional activation of AMPK by these compounds in HEK293 cells, levels of its downstream target, phosphorylated acetyl-CoA carboxylase (pACC), were also determined, confirming a good correlation between the levels of pAMPK and pACC (Figure 2). On the contrary, compound IND1310 did not show any property as an AMPK activator (data not shown).

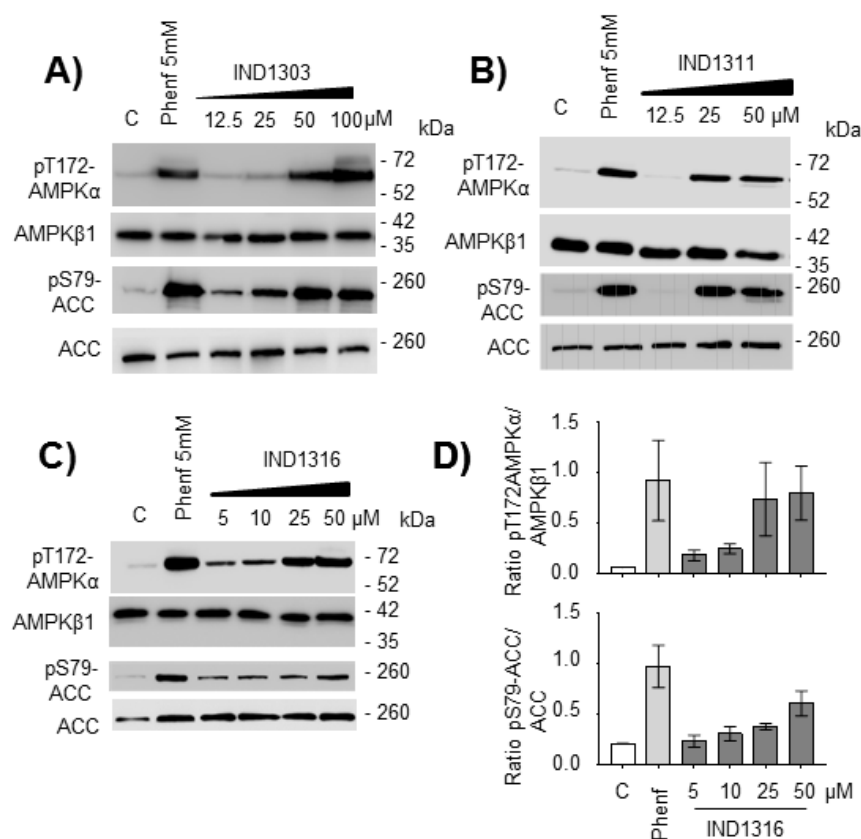**Figure 2:** AMPK activation properties of different indole compounds [IND1303 (A), IND1311 (B), and IND1316 (C)]. HEK293 cells growing in KHR/Glu minimal media (see Material and Methods) were treated with the indicated concentration of different

indole compounds for 1 hour and the activation of the endogenous AMPK complex was assessed by checking the phosphorylation status of the AMPK catalytic subunit (pT172-AMPKα) and the phosphorylation of a canonical substrate of the AMPK complex (pS79-ACC). The levels of AMPKβ1 and ACC were used as loading controls. Cells treated with 5 mM phenformin were used as a positive control of AMPK activation. C lane corresponds to untreated cells. Representative blots of three independent experiments are shown. (D) Quantification of the bands for the IND1316 product was performed as described in Materials and Methods. Intensity of the bands was referred to the one observed in the Phenformin treated samples.

In these initial investigations, our preliminary structure-activity relationship studies (SAR) revealed how the presence at C2 of a carboxylic group in the indole ring (Figure 1) seems to be essential for AMPK activation in HEK293 cells. The absence of activity in compound IND1310, which contained an ester group at this position, but the full activity of the same structure when there was a carboxylic group in that position (compound IND1311), reinforced this evidence. In the case of compounds IND1303 and IND1316, both with a carboxylic group at C2, the different substitution pattern of aromatic residues at the C3 position may affect their physicochemical properties and could account for the differences observed in the corresponding AMPK activation.

In parallel with the AMPK activation assays, cell viability studies were performed in HEK293 cells, as described in Materials and Methods (Figure 3). We observed that compounds IND1303, IND1311, and IND1316 did not manifest major cell toxicity up to 100 μM. However, at 200 μM compound IND1311 exhibited high toxicity in comparison to the rest of the compounds. At this higher concentration, compound IND1316 was the least toxic compound.
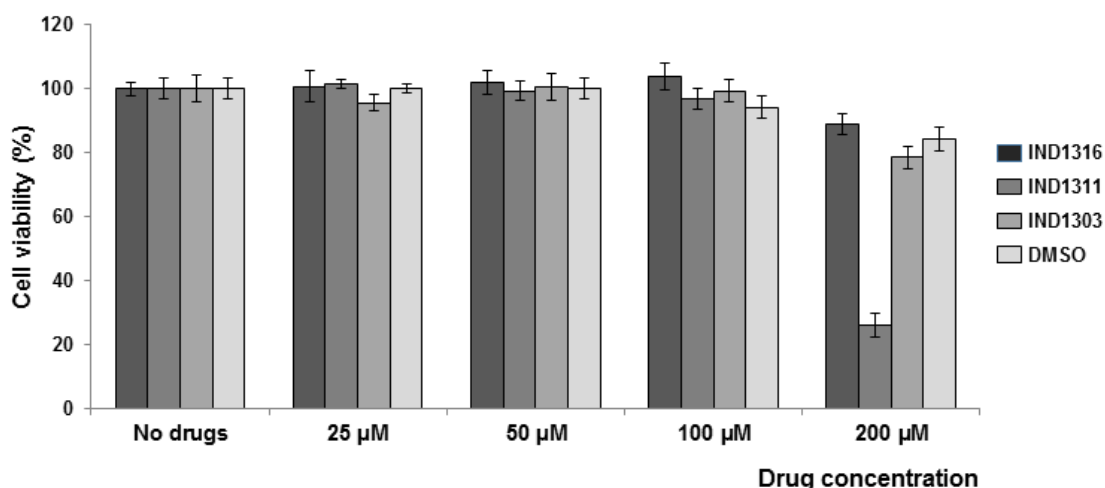
Figure 3: Cell viability assays of different indole compounds (IND1303, IND1311, and IND1316). HEK293 cells were treated with different concentrations of the indicated indole compounds and cell viability was assessed as indicated in Materials and Methods. Since the compounds were dissolved in DMSO, a sample containing this dissolvent was used as a negative control.

Drug-likeness calculations

In order to evaluate the potential as future drug candidates, *in silico* predictions of properties related to Absorption, Distribution, Metabolism, Excretion (ADME) of IND1303, IND1311, and IND1316 active compounds were carried out using the QikProp 3.5 program, integrated into Maestro (Schrödinger LLC, New York, USA). To estimate the bioavailability of the compounds, we employed a combination of oral absorption and permeability parameters taking into account the following descriptors: predicted aqueous solubility (QPlogS), conformation-independent predicted aqueous solubility (CLQPlogS), and predicted human oral absorption (%HumanOralAbsortion) to assess oral absorption. To include permeability issues, we employed the predicted apparent Caco-2 cell permeability values (QPPCaco) because it could be considered as a

model for the gut-blood barrier. Finally, to integrate information about the blood-brain barrier (BBB) permeability, we used the predicted brain/blood partition coefficient (QPlogBB) as a measure of access to the central nervous system. Moreover, the predicted apparent MDCK cell permeability (QPPMDCK) was also selected as an additional criterion, since it is considered a good mimic for BBB in the cases of compounds acting as non-active transporters. The combined results of both calculated parameters, QlogBB and QPPMDCK, suggest that indole compounds show an adequate cellular permeability to act as active compounds at CNS level. Finally, metabolic issues were also assessed by predicting the number of likely metabolic steps (#metab) as a measure of the likelihood of a compound to easily gain access to the target site after entering the bloodstream.

An analysis in detail of the results depicted in Table 1 showed that BBB permeability values of the compound candidates were consistent with the range predicted by QikProp. In addition, the fact that these compounds were able to activate AMPK in HEK293 cells indicates that they were able to cross the cell membrane in these cells. However predicted bioavailability values of compound IND1303 and IND1311 fell outside the range of 95% of known oral drugs, suggesting that compound IND1316 has a better suitable drug profile in terms of bioavailability and BBB permeability predictions.

Descriptor		IND1303	IND1311	IND1316
Bioavailability	QPlogS[a]	-5.123	-7.090	-5.949
	CIQPlogS[b]	-5.787	-8.139	-6.214
	%HumanOralAbsorption[c]	85.952	95.420	85.392

	QPPCaco[d]	91.988	282.733	214.357
Blood-brain barrier permeability	QPlogBB[e]	-1.088	-0.766	-0.825
	QPPMDCK[f]	47.721	160.617	119.077
Metabolism	#metab[h]	1	2	2

Table 1. Calculated physicochemical descriptors of IND1303, IND1311 and IND1316 compounds. a) QPlogS: Predicted aqueous solubility, logarithm of aqueous solubility in g/dm^3 [range for 95% of drugs is −6.0 to 0.5]; b) CIQPlogS: Conformation-independent predicted aqueous solubility, log S. S in mol dm^{-3} [range –6.5 – 0.5]; c) %HumanOralAbsorption: [<25% is poor]; d) QPPCaco: Predicted apparent Caco-2 cell permeability in nm/sec [range for 95% of drugs is <5 low, >100 high]; e) QPlogBB: Predicted brain/blood partition coefficient [range for 95% of drugs is −3.0 to 1.0]; f) QPPMDCK: Predicted apparent MDCK cell permeability in nm/sec [<25 poor]; h) #metab: Number of likely metabolic reactions [range for 95% of drugs: 1-8].

Taking together all the results presented so far, the IND1316 derivative resulted in the most promising candidate, since it activated AMPK at low concentrations and had no toxic effect even at high concentrations (200 µM). Moreover, IND1316 showed an adequate *in silico* druggability profile. Thus, we selected this compound for further studies.

Performance of IND1316 as an activator of AMPK

In order to understand the mechanism of action of IND1316, we performed binding studies by surface plasmon resonance (SPR) and compared them with those obtained for

the direct AMPK activator A-769662 (Table 2). Our results indicate that at 100 μM, IND1316 binds to the AMPK complex used in the assay (AMPK α1/β1/γ1) with a strength of resonance units (RU) of 5.2 which is lower than the one from A-769662 (31.7 RU), but higher than the one from the negative control β-cyclodextrin (1.6 RU). These results indicated a weak interaction of IND1316 with the AMPK complex *in vitro*.

Compound	Binding at 100 μM (RU)[a]	% Activation at 30 μM[b]
IND1316	5.2	-62.0 ± 2.7
A-769662	31.7	394 ± 76
β-cyclodextrine	1.6	nd

Table 2: *In vitro* performance of IND1316 as an AMPK activator. The *in vitro* performance of IND1316 was assessed on the AMPK α1/β1/γ1 complex. (a) Data is the mean ± SD of 3-6 independent experiments. (b) Data is the mean ± SD of the three independent experiments. nd: Not determined.

In addition, we checked the performance of IND1316 and A-769662 at 30 μM on the *in vitro* activity of the AMPK complex (Table 2). We found a rather inhibitory activity of the IND1316 instead of the regular activation profile observed with the A-769662 drug. These results pointed out a paradoxical mode of action of IND1316 on the AMPK complex, since on the one hand it activates AMPK in cells (Figure 2), whereas on the other hand, it shows an inhibitory profile *in vitro* (Table 2).

Finally, we analyzed by western blot the ability of IND1316 to activate different signaling pathways and compare it with the effect of phenformin and A-769662, an indirect and direct activator of AMPK, respectively. As it can be observed in Figure 4, IND1316 at 50 µM was able to induce the phosphorylation of AMPK at Thr172 as described above (Figure 2). Similar effects were observed upon the treatment with 5 mM phenformin, but none of the concentrations used for the A-769662 was able to induce this phosphorylation, which is in agreement with previous results described in the literature as A-769662 is a direct activator of AMPK.[6] However, the three of them were able to stimulate the phosphorylation of ACC at Ser79. Additional AMPK substrates such as raptor (Ser792), and ULK1 (Ser555) were more efficiently phosphorylated by IND1316 and phenformin than with A-769662. Moreover, IND1316 was able to stimulate the phosphorylation of MAP-kinases such as p38 (at Thr180/Tyr182) and JNK (at Thr183/Tyr185). In the case of A-769662, the drug was able to induce the phosphorylation of JNK and p38, although the latter at minor extent and phenformin produced only minor changes in the phosphorylation of these two MAPKs. These results may suggest that IND1316 may have a broader activation profile on different protein kinases.
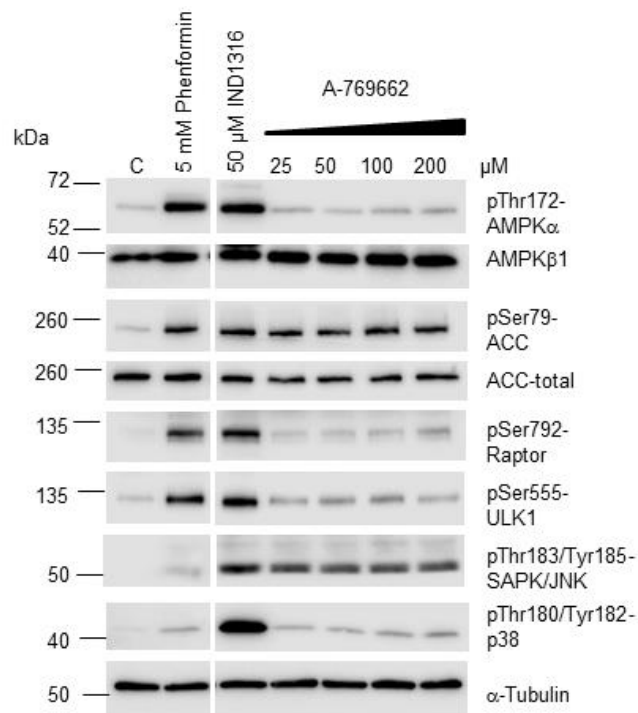
Figure 4: IND1316 activates additional protein kinases. HEK293 cells growing in KHR/Glu minimal media (see Material and Methods) were treated with the indicated concentration of different compounds (IND1316, phenformin, and A-769662) for 1 hour and the activation of the endogenous AMPK complex was assessed by checking the phosphorylation status of the AMPK catalytic subunit (pT172-AMPKα) and the phosphorylation of canonical substrates of the AMPK complex (pS79-ACC, pS792-Raptor, and pS555-ULK1). The levels of AMPKβ1, ACC and tubulin were used as loading controls. In addition, the phosphorylation status of two MAP kinases was also assessed (pThr180/Tyr182-p38 and pThr183/Tyr185-JNK). The C lane corresponds to untreated cells. Representative gels of three independent experiments are shown. (Figure 4 is a composition of two areas of the same gel; the full gel is shown as Supplementary Fig. S1).

IND1316 reduces phenotypes associated with the expression of polyQ in *C. elegans*

It has been recently shown that AMPK activation is beneficial in different models of polyQ toxicity and/or HD.[10,11,12,13,15] Since IND1316 is such a good activator of AMPK *in vitro*, we sought to test whether culturing worms on this substance would alter the dynamics of aggregation of polyQs. With this aim, we used a *C. elegans* strain that expresses 40 CAG repeats in frame with the yellow fluorescent protein (40Q::YFP) in muscle cells.[16] These worms show an age-dependent aggregation pattern of the polyQ-containing protein, i.e. young animals (L1, L2, and L3 larval stages) show expression of the 40Q::YFP which appears non-aggregated, while L4 larvae, young adults, and older adults show an increasing accumulation of inclusion bodies, which is an indirect consequence of the aggregation process.[16] Interestingly, worms treated with 50 µM IND1316 showed a substantial reduction in the number of inclusion bodies (Figure 5A). This result is in agreement with the profile exhibited by other AMPK activators such as metformin,[10] suggesting again that activation of AMPK induces pathways of misfolded protein clearance.

Next, we sought to find out whether the effect of IND1316 in reducing polyQ aggregates, may have an impact on the function of neurons impaired by these toxic molecules. In this case, we used worms expressing 112 CAG repeats in frame with TdTomato in mechanosensory neurons.[10] These worms show reduced mechanosensation as observed by a reduction in the touch response (see Material and Methods). Culturing these animals in the presence of AMPK activators such as metformin, an increase in mechanosensation is observed.[10] The treatment with 50 µM IND1316 improved substantially the touch response in 112Q::TdTomato animals (Figure 5B), suggesting that this compound could be used to reduce toxicity induced by polyQ and/or mutant huntingtin.
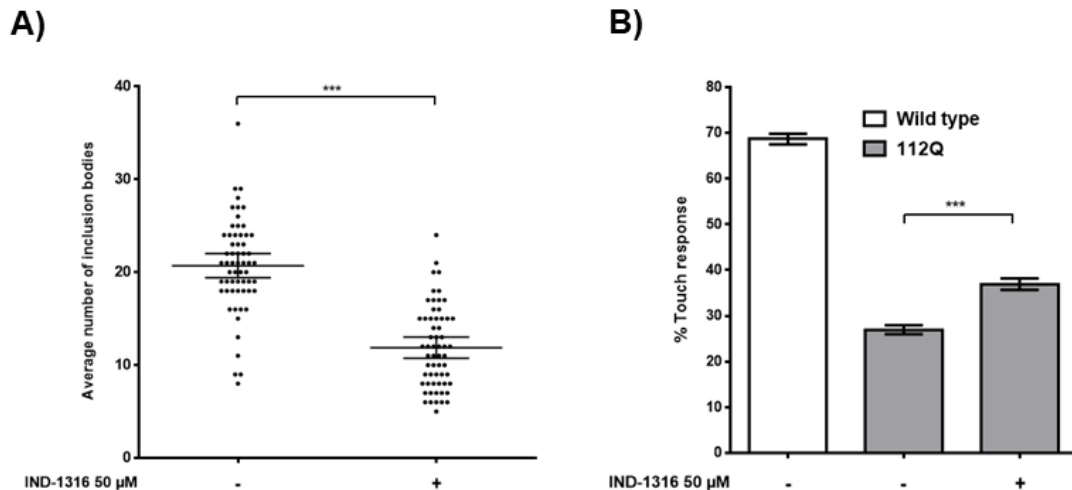
Figure 5: IND1316 can reduce the rate of aggregation of polyQs and restore neuronal functionality. A) IND1316 reduces the average number of inclusion bodies, which is a direct result of the final steps of aggregation, in worms expressing 40Q::YFP fusion in muscle cells. B) IND1316 restores functionality in mechanosensory neurons, based on a touch assay phenotype, in worms expressing 112Q::TdTomato fusion (see Materials and Methods).

Neuroprotective effect of IND1316 on a mouse model of HD (zQ175).

After the positive results of IND1316 in an *in vivo* model of polyQ toxicity (*C. elegans*), we decided to study in a mouse model of HD (zQ175; a mouse carrying a humanized exon 1 of *HTT* gene containing around 190 CAG tandem repeats,[17]) if the administration of IND1316 improved the neuropathological phenotype present in these animals. Male wild type and heterozygous zQ175 mice of three months of age were treated with 36 mg/L of IND1316 dissolved in the drinking water, for three months. During this period, we checked that a similar volume of water was drunk by wild type and zQ175 mice, and no differences in body weight or other health parameters were observed among treatment groups and control animals. At the beginning of the

treatment (pre-treatment) and after three months (post-treatment), animals were subjected to a battery of behavioral tests to check whether IND1316 had a beneficial effect on the abnormal behavior of zQ175 mice. As some of the earliest deficits observed in zQ175 mice are neuropsychiatric changes, the tail suspension test (TST) was performed to assess depression-related behaviors.[18,19] This test is used to model behavioral despair by measuring immobility time during testing. As shown in Fig. 6A, heterozygous zQ175 mice of three months of age (pre-treatment) displayed a relative increase in immobility time in the TST in comparison to wild type animals (150.7 +/- 33.9 in zQ175 vs 100.0 +/- 13.1 in wild type mice; ***$p<0.001$, n:8). This difference was maintained in untreated animals after the treatment period (post-treatment) (147.9 +/- 30.8 in zQ175 vs 100.0 +/- 24.66 in wild type mice; ***$p<0.001$, n:8). However, zQ175 mice treated with IND1316 displayed a reduction in the immobility time (111.32 +/- 26.20) that was statistically significant in comparison to untreated zQ175 mice of the same age (*$p<0.05$, n:8). Therefore, IND1316 reduced the immobility time in zQ175 mice to values similar to wild type animals.

To characterize the effect of IND1316 on motor coordination, we subjected the animals to the beam balance test (BBT). At the beginning of the treatment, untreated zQ175 mice took longer to cross the 12 mm wide beam respect to wild type animals (16.79 +/- 3.39 sec in zQ175 vs 10.50 +/- 1.56 sec in wild type; ***$p<0.001$, n:8) and in the 5 mm wide beam (22.08 +/- 16.00 sec in zQ175 vs 16.00 +/- 1.66 sec in wild type; ***$p<0.001$, n:8) (Figure 6B). After the treatment period, we observed statistically significant differences between untreated zQ175 and wild type animals but only in the 5 mm wide beam. Untreated zQ175 mice took longer time to cross the beam than wild type (23.08 +/- 3.49 sec vs 15.50 +/- 1.92 sec respectively; ***$p<0.001$, n:8). However, zQ175 mice treated with IND1316 displayed a reduction in the time to cross the 5 mm

wide beam (18.21 +/- 2.87), being this reduction statistically significant in comparison to the values of the untreated zQ175 mice of the same age (*p<0.05; n:8) (Fig. 6B). Therefore, treatment with IND1316 ameliorated the motor coordination defect present in zQ175 mice.
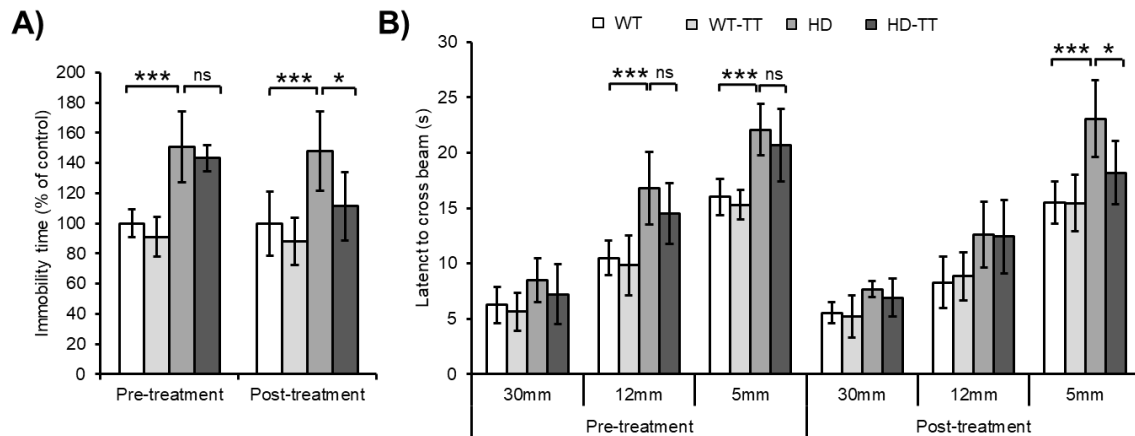

Figure 6: IND1316 treatment ameliorates the neuropsychiatric and motor behavior phenotype in heterozygous zQ175 mice (HD). Different behavioral tests were analyzed in three-month-old mice (pretreatment) and after three months of treatment (six-month-old; posttreatment). A) HD and control mice were subjected to the tail suspension test, and the immobility time was measured (see Materials and Methods). HD mice showed a depressive state as early as three months of age, which was worse in six-month-old animals. However, when the mice were treated with IND1316, their depression-related behavior became similar to that in WT animals (*p<0.05, n:8). B) HD and control animals were subjected to the beam balance test. The time to cross each beam was recorded. At three months of age, HD mice exhibited difficulties crossing beams of different widths compared to WT animals (12 mm: ***p<0.001 and 5 mm: ***p<0.001, n:8). In contrast, HD mice treated with IND1316 showed a reduced latency to cross the beam in comparison to non-treated mice (*p<0.05, n:8), and the values were similar to those for WT controls in the case of the 5 mm width beam. Values are the mean +/-

standard deviation. Statistical analysis was performed using two-way ANOVA following Tukey's posthoc test to multiple comparisons.

Next, we analyzed whether the treatment with IND1316 affected the activation of AMPK in the brain of the animals. As indicated in Figure 7, by western blot analyses of brain crude extracts we observed higher levels of pT172-AMPKα and pS79-ACC in the brains from zQ175 mice treated with IND1316 in comparison to untreated HD mice. These results indicated that IND1316 had reached the brain and activated AMPK in that organ. We also noticed that untreated HD mice had higher activated forms of AMPK in comparison to controls.
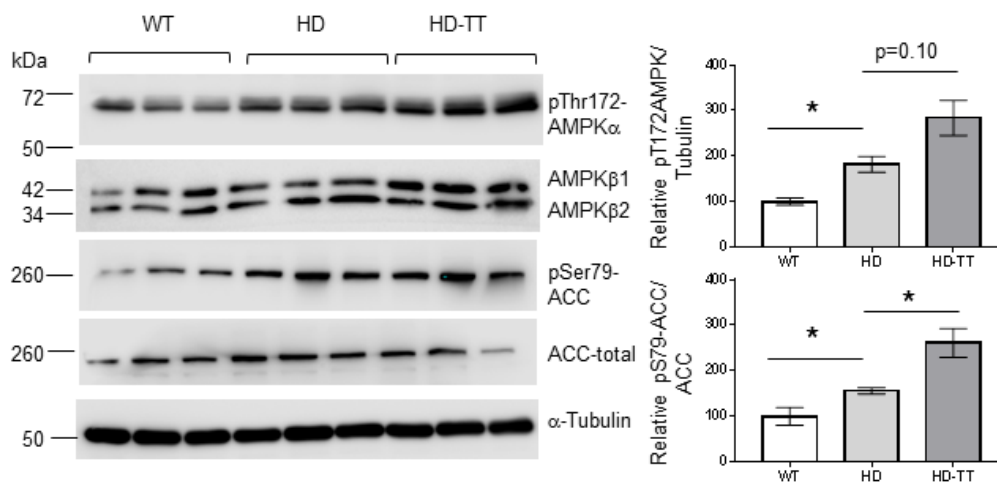

Figure 7: IND1316 can activate AMPK in the brain of zQ175 treated mice. Crude extracts from the brain of IND1316 treated and untreated mice were analyzed by western blot and the activation of the endogenous AMPK complex was assessed by checking the phosphorylation status of the AMPK catalytic subunit (pT172-AMPKα) and the phosphorylation of the canonical substrate of the AMPK complex (pS79-ACC). The levels of AMPKβ1/β2, ACC, and tubulin were used as loading controls. Quantification of the bands was performed as described in Materials and Methods.

Intensity of the bands was referred to the one observed in control mice. Statistical significance is indicated as *p<0.05, n: 3.

Then, we performed an immunohistological analysis of the brain of treated and untreated animals. First, brain slices were immunostained with anti-mHtt antibodies (see Materials and Methods). Although we observed an increase in the number of mHtt inclusions in untreated zQ175 mice in comparison to controls (not shown), zQ175 mice treated with IND1316 showed similar levels of mHtt aggregates as untreated animals in either hippocampus or striatum (Figure 8A, Supplementary Fig. S2A). We also performed an immunofluorescence analysis using anti-GFAP, a marker of reactive astrocytes, and anti-Iba1, a marker of reactive microglia. Again, in both hippocampus and striatum, we did not observe differences in the intensity of the GFAP signal (Figure 8B, Supplementary Figure S2B) or the number of activated microglia (Figure 8C, Supplementary Figure S2B) between zQ175 mice treated or untreated with IND1316. Finally, we analyzed by qRT-PCR the expression levels of two pro-inflammatory mediators, namely TNFα and IL-1β, and observed that the treatment with IND1316 did not affect the levels of these two markers in comparison to untreated HD mice (Figure 8D). All these results suggested that IND1316 did not have a major effect on the inflammatory markers analyzed in this study.
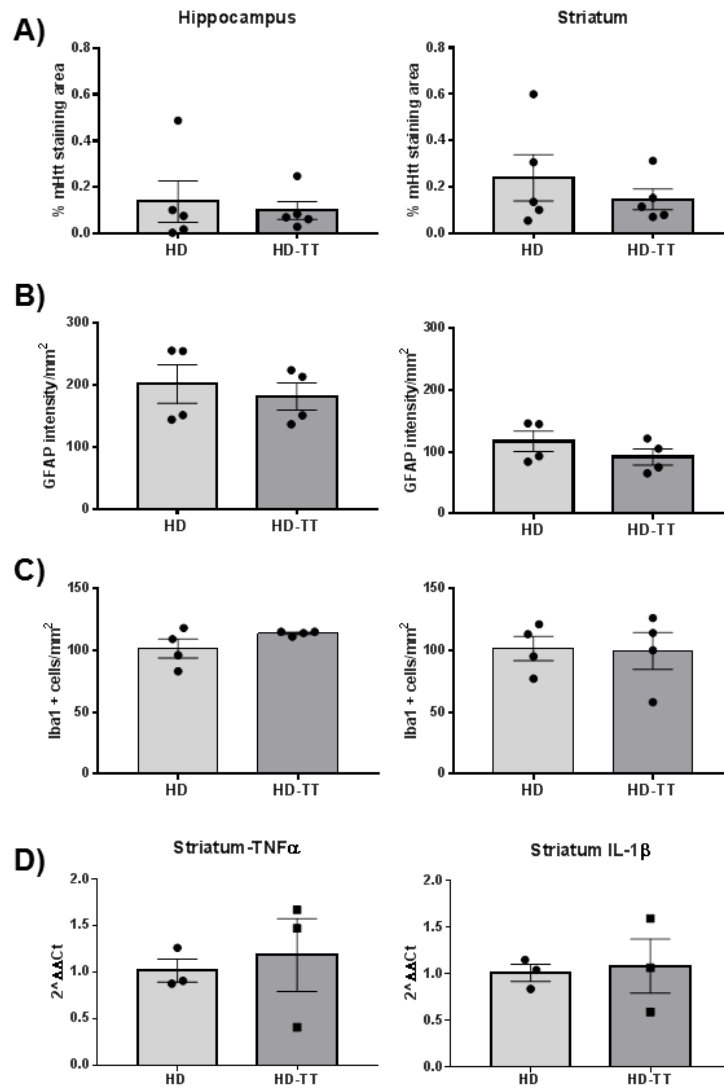
Figure 8: IND1316 does not affect the number of mHtt aggregates or the presence of neuroinflammatory markers in zQ175 mice. A) Brain samples from zQ175 treated (HD-TT) and untreated (HD) mice were analyzed by immunohistochemistry using anti-mHtt antibodies. The intensity of the signal corresponding to the mHtt aggregates was recovered in two areas of the brain, hippocampus, and striatum. No statistically significant differences were found (n: 5). Immunofluorescence analysis with anti-GFAP (B) and with anti-Iba1 (C) showed no differences in the intensity of these two neuroinflammatory markers in samples from zQ175 treated and untreated animals (n: 4). (D) Expression levels of TNFα and IL1β in the striatum of treated and untreated zQ175 mice were assessed by qRT-PCR as indicated in Materials and Methods. Values

are expressed as $2^{\Delta\Delta Ct}$ respect to the housekeeping GAPDH gene. No major changes in the expression were observed (n: 3).

DISCUSSION

Activators of AMPK have been shown to alleviate phenotypes in *in vitro* and *in vivo* models of HD. [9,10,11,15,20] In this regard, treatments with metformin, a well-known indirect activator of AMPK, were able to rescue motor and other behavioral and molecular phenotypes in two different mice models of HD.[10,15] Moreover, in a cross-sectional study, some authors observed that the intake of metformin, by patients of HD that also were type 2 diabetics, associated with better marks in cognitive tests.[13]

Indole structure is a privileged scaffold in medicinal chemistry, because using them, it is possible to expand the available drug-like chemical space and drive more effective drug discovery programs. In particular, it has proved to be relevant in reducing polyQ toxicity aggregation. Indole derivatives NC001-8 or NC001-9 have been used to treat polyQ toxicity in *in vitro* and *in vivo* models of spinocerebellar ataxias.[21,22,23] In contrast to IND1316, which strongly activates AMPK, the mechanism induced by these molecules is AMPK-independent, in principle, and involves the mobilization of chaperones.[21,22,23] For example, AMPK activity reduces the expression of HSF1 and HSP70 in models of cancer,[24] therefore, it is unlikely that indole NC001-8 is acting through AMPK. However, culturing cells expressing TATA box binding protein with expansions of polyQs with the indole species NC001-9 can increase the expression of HSPB1, which in turn reduces aggregation of these polyQ-containing proteins *in vitro*, and ameliorates motor behavior in mice.[23] Interestingly, this chaperone is a downstream effector of AMPK in muscle cells,[25] which raises the possibility that the beneficial effect produced by this indole may require AMPK function.

Herein we show that IND1316, a new synthetic indole, can activate *in cells* AMPK in a dose-dependent manner (Figure 2). In addition, we provide evidence that IND1316 induces the activation of different MAPK pathways (p38 and JNK; Fig. 4). *In vivo*, we have tested the beneficial effect of IND1316 in two animal models of HD, namely worms and mice. On the one hand, IND1316 can reduce polyQ aggregation and neuronal impairment *in vivo* in *C. elegans*. On the other hand, it ameliorates the neuropsychiatric phenotype of the zQ175 HD mouse model. However, in HD mice, we did not observe any effect of IND1316 at the levels of mHtt inclusions or in the levels of neuroinflammatory markers that accompany HD. Long ago, it was suggested that mHtt aggregation may not be a good biomarker to predict neuronal death in HD[26], because phenotypes and aggregation of mHtt do not always progress in parallel. For example, Miller and co-workers rescued insulin-related phenotypes by inducing immunization against huntingtin in R6/2 mice[27]. However, these authors failed to observe a reduction of mHtt aggregation in pancreatic cells[27]. These results agree with work performed in *Drosophila* in which the authors showed that aggregation of human mHtt is independent of animal viability[28]. Furthermore, these apparently conflicting findings (i.e. phenotypic changes independent of the progression of aggregation), have also been observed in mice models of Parkinson disease. In this regard, Arawaca and colleagues found that treating mice overexpressing α-synuclein, with zinisamide, resulted in cell protection of nigrostriatal dopamine neurons,[29] although no reduction of α-synuclein aggregates was observed. In our case, the differences in the removal of mHtt aggregates between worms and mice could be explained if we have in mind that the worms were treated from the first larval stage, the so-called L1 stage (from four larval stages). This means that they have grown through nearly their entire developmental cycle under the effects of the drug. Aggregation in worms occurs

gradually, starting to be substantial at the fourth larval stage. This means that IND1316 may be preventing the appearance of the aggregates way before they start to nucleate and grow. In contrast, the zQ175 mice were treated with the indole species from the 3-month of age, from which the animals already show clear signs of mHtt aggregation.[30,31] Hence, the mice have already growing aggregates, at the age of 3-months, and once they are formed it is difficult (if not impossible) to reduce them. This, together with the fact that the indole has a subtle effect on biomarkers, makes the aggregates of mHtt grow freely in the treated mice.

Having all this information in mind, we hypothesize that the beneficial effects of IND1316 on zQ175 HD mice could be due to the action of the compound on alternative pathways not related to neuroinflammation. In this sense, we show in this study that IND1316 can induce the phosphorylation of two MAP kinases (p38 and JNK). Perhaps the combined activation of AMPK and MAPK in the brain is related to the beneficial effects we observed in the behavioral tests.

CONCLUSIONS

In this work, we present the synthesis and activation studies of a novel family of AMPK activators. Based on the predicted pharmacokinetic properties and toxicity studies, we selected IND1316 as a good candidate for proof of efficacy studies, since we found a balance between druggability and toxic profiles. By using *C. elegans* models of polyQ toxicity, we demonstrated that IND1316 was able to improve the mechanosensory response, probably by reducing polyQ aggregation and neuronal impairment. We would like to point out that IND1316 performance was obtained at low concentration doses (50 μM), 40 times lower than the one required to observe the same effect with metformin (2 mM),[10] which reveal the high neuroprotective effect of IND1316 in this model.

Moreover, the treatment of the zQ175 mouse model of HD with IND1316 demonstrated its efficacy in ameliorating different behavioral tests that are affected in this model. In summary, we propose that IND1316 could be a promising lead compound for the development of new HD treatments.

MATERIAL AND METHODS

Chemistry

All reagents were of commercial quality. Solvents were dried and purified by standard methods. Analytical TLC was performed on aluminum sheets coated with a 0.2 mm layer of silica gel 60 F254. Silica gel 60 (230-400 mesh) was used for flash chromatography. Analytical HPLC-MS was performed on Waters equipment coupled to a single quadrupole ESI-MS (Waters Micromass ZQ 2000) using a reverse-phase SunFire C18 4.6 × 50 mm column (3.5 μm) at a flow rate of 1 mL/min and by using a diode array UV detector. Mixtures of CH_3CN and H_2O were used as mobile phases (gradient of 15−95% of acetonitrile in water, as indicated in each case). HRMS (EI+) was carried out on Agilent 6520 Accurate-Mass Q-TOF LC/MS equipment. NMR spectra were recorded on a Bruker-AVANCE 300, a Varian-INOVA 400, and VARIAN SYSTEM-500 spectrometer. Melting points were determined on a Mettler MP70 apparatus and are uncorrected.

1-benzyl-3-iodo-1H-indole-2-ethyl carboxylate (3). To a solution of 3-iodo-1H-indole-2-ethyl carboxylate (2)[14] (315 mg, 1 mmol) in DMF (3 mL) at 0°C, NaH (26.4 mg, 1.1 mmol) was added. Next, benzyl bromide (223 mg, 1.3 mmol) was slowly added. The reaction was stirred at room temperature for 2 hours and then, the mixture was concentrated *in vacuo*, and water (10 mL) was added. The mixture was extracted with AcOEt (2 x 15 mL). The organic phase was dried over anhydrous sodium sulfate,

filtered and concentrated *in vacuo*. The crude was purified by chromatographic column using Hex/AcOEt (10:1) as eluent to afford, after concentration and high vacuum-drying, the corresponding aryl products 315 mg (78%) of a white solid. MS (ES, positive mode): m/z 405 (95%) (M + H)$^+$. ^{1}H NMR (CDCl$_3$) δ 7.53 (d, J = 8.0 Hz, 1H), 7.36 – 7.10 (m, 5H), 6.94 (dd, J = 6.8, 1.5 Hz, 2H), 5.73 (s, 3H), 4.30 (q, J = 7.1 Hz, 3H), 1.31 (t, J = 7.1 Hz, 5H). ^{13}C NMR (CDCl$_3$) δ 13.2, 48.0, 60.3, 66.8, 109.9, 120.7, 123.0, 125.1, 125.3, 126.2, 127.4, 127.6, 129.4, 136.8, 137.8, 160.1.

1-benzyl-3-(2'-hydroxy-[1,1'-biphenyl]-4-yl)-1H-indole-2-ethyl carboxylate (4) IND1310. To a solution of 1-benzyl-3-iodo-1H-indole-2-ethyl carboxylate (3) (290 mg, 0.72 mmol), Pd(dppf)Cl$_2$ (26 mg, 0.036 mmol) and 4'-(4,4,5,5-tetramethyl-1,3,2-dioxoborolan-2-yl) biphenyl-2-ol (255 mg, 0.86 mmol) in a solvent mixture of toluene:ethanol:water:1,4-dioxane 1:3:6:10 (20 mL), an aqueous solution (5 mL) of K$_2$CO$_3$ (398 mg, 2.88 mmol) was slowly added while stirring under argon. After 3 hours at 85°C, the mixture was concentrated in vacuo, and water (10 mL) was added. The mixture was extracted with AcOEt (3 x 10 mL). The organic phase was dried over anhydrous sodium sulfate, filtered and concentrated in vacuo. The crude was purified by chromatographic column using CH$_2$Cl$_2$: MeOH (50:1) as eluent to afford, after concentration and high vacuum-drying, 305 mg (95%). MS (ES, positive mode): m/z 447 (95%) (M+1)$^+$. ^{1}H NMR (DMSO-d_6) δ 9.59 (s, 1H), 8.05 – 6.45 (m, 17H), 5.79 (s, 2H), 4.12 (q, J = 6.5 Hz, 2H), 1.00 (t, J = 7.1, 6.5 Hz, 3H).^{13}C NMR (DMSO-d_6) δ 13.8, 47.8, 55.3, 61.0, 111.7, 116.5, 119.9, 121.3, 121.5, 123.8, 125.0, 125.7, 126.2, 126.7, 127.5, 127.8, 128.8, 128.9, 129.0, 130.0, 130.6, 132.3, 137.5, 138.1, 138.7, 154.8, 162.2.

3-(2'-hydroxy-[1,1'-biphenyl]-4-yl)-1H-indole-2-ethyl carboxylate (6). To a solution of 3-iodo-1H-indole-2-ethyl carboxylate (2) (87 mg, 0.27 mmol), Pd(dppf)Cl$_2$ (10 mg,

0.01 mmol) and 4'-(4,4,5,5-tetramethyl-1,3,2-dioxoborolan-2-yl) biphenyl-2-ol (98 mg, 0.33 mmol) in a solvent mixture of toluene:ethanol:water:1,4-dioxane 1:3:6:10 (20 mL), an aqueous solution (5 mL) of K_2CO_3 (150 mg, 1.08 mmol) was slowly added while stirring under argon. After 18 hours at 85°C, the mixture was concentrated in vacuo, and water (10 mL) was added. The mixture was extracted with AcOEt (3 x 10 mL). The organic phase was dried over anhydrous sodium sulfate, filtered and concentrated in vacuo. The crude was purified by chromatographic column using CH_2Cl_2: MeOH (20:1) as eluent to afford, after concentration and high vacuum-drying, 56 mg (60%). MS (ES, positive mode): m/z 357 (96%) $(M+1)^+$. ^{1}H NMR (DMSO-d_6) δ 11.96 (s, 1H), 9.63 (s, 1H), 8.18 – 6.05 (m, 12H), 4.30 (d, J = 7.1 Hz, 2H), 1.28 (t, J = 7.1 Hz, 3H). ^{13}C NMR (DMSO-d_6) δ 14.4, 60.7, 113.1, 116.5, 119.9, 120.9, 121.1, 122.8, 123.1, 125.5, 127.2, 127.9, 128.8, 130.4, 130.7, 132.1, 136.6, 137.5, 154.8, 161.7.

3-(3-benzyloxyphenyl)-1H-indole-2-ethyl carboxylate (7). To a solution of ethyl 3-iodo-1H-indole-2-carboxylate (2) (150 mg, 0.48 mmol), Pd(dppf)Cl₂ (18 mg, 0.02 mmol) and (3-benzyloxyphenyl)boronic acid (102 mg, 0.57 mmol) in a solvent mixture of toluene:ethanol:water:1,4-dioxane 1:3:6:10 (20 mL), an aqueous solution (5 mL) of K_2CO_3 (265 mg, 1.92 mmol) was slowly added while stirring under argon. After 2 hours at 85°C, the mixture was concentrated in vacuo, and water (20 mL) was added. The mixture was extracted with AcOEt (3 x 20 mL). The organic phase was dried over anhydrous sodium sulfate, filtered and concentrated in vacuo. The crude is purified by column chromatography (CH_2Cl_2:MeOH 50:1). 135 mg (77%) are obtained as a white solid. MS (ES, positive mode): m/z 371 (94%) $(M+1)^+$. ^{1}H NMR (DMSO-d_6) δ 11.91 (s, 1H), 7.55 – 6.97 (m, 13H), 5.16 (s, 2H), 4.23 (q, *J* = 7.1 Hz, 3H), 1.19 (t, *J* = 7.1 Hz, 3H). ^{13}C NMR (DMSO-d_6) δ 161.75, 157.91, 137.32, 136.27, 134.91, 129.41, 128.90,

128.23, 127.74, 126.84, 125.73, 123.42, 122.87, 122.60, 121.12, 120.79, 117.01, 113.98, 112.92, 69.48, 60.96, 14.14.

General procedure for the synthesis of the carboxylic acids 5 (IND1311), 8(IND1303), and 9 (IND1316). To a solution of the corresponding ester (1 eq) in EtOH: H_2O (20 mL), KOH (4 eq.) dissolved in H_2O was added. After stirring at 100°C for 3 hours, HCl 1N (2 mL) was added. The resultant solid was filtrated and dried under reduced pressure to give the corresponding acids.

1-benzyl-3-(2'-hydroxy-[1,1'-biphenyl]-4-il)-1H-indole-2-carboxylic acid (5, IND1311). Prepared from 4 (200 mg, 0.45 mmol) and KOH (75 mg, 1.34 mmol) by following the general procedure described for 3-aryl-1*H*-indole-2-carboxylic acid. Yield 125 mg (66%) of white solid. HPLC (SunFire): t_R= 7.0 min. MS (ES, positive mode): 419 (95%) (M + H)$^+$ Mp 181°C-182°C. ^{1}H NMR (DMSO-*d6*) δ 13.11 (s, 1H), 9.64 (s, 1H), 8.27 – 6.53 (m, 16H), 5.86 (s, 2H). ^{13}C NMR (DMSO-*d6*) δ 47.6, 111.6, 116.5, 119.8, 121.3, 122.9, 125.3, 126.4, 126.8, 127.4, 127.7, 128.9, 130.0, 130.6, 132.7, 137.3, 137.9, 149.4, 154.8, 163.8. HRMS (EI+) m/z ([M]$^+$) calcd for $C_{28}H_{21}NO_3$ 419.15214; found 419.15219.

3-(2'-hydroxy-[1,1'-biphenyl]-4-yl)-1H-indole-2-carboxylic acid (8, IND1303). Prepared from 6 (200 mg, 0.56 mmol) and KOH (94 mg, 1.68 mmol) by following the general procedure described for 3-aryl-1*H*-indole-2-carboxylic acid. Yield 90 mg (50%) of white solid. HPLC (SunFire): t_R= 6.2 min. MS (ES, positive mode): 329 (99%) (M + H)$^+$ Mp 216°C-217°C. ^{1}H NMR (DMSO-*d6*) δ 11.82 (s, 1H), 8.05 – 6.48 (m, 12H). ^{13}C NMR (DMSO-*d6*) δ 112.9, 116.5, 119.8, 120.6, 120.9, 122.2, 123.9, 125.1, 127.4, 127.9, 128.8, 130.4, 130.6, 132.4, 136.4, 137.2, 154.8, 163.2. HRMS (EI+) m/z ([M]$^+$) calcd for $C_{21}H_{15}NO_3$ 329.10519; found 329.10591.

3-(3-(Benzyloxy) phenyl)-1H-indole-2-carboxylic acid (9, IND1316). Prepared from **7** (95 mg, 0.26 mmol) and KOH (51 mg, 0.77 mmol) by following the general procedure described for 3-aryl-1*H*-indole-2-carboxylic acid. Yield 18 mg (21%). HPLC (SunFire): t_R= 6.76 min. MS (ES, positive mode): 344 (M+1)$^+$. Mp 150ºC-152ºC. ^{1}H NMR (300 MHz, DMSO-d_6) δ 12.87 (s, 1H), 11.81 (s, 1H), 7.49- 6.95 (m, 13H), 5.15 (s, 2H). ^{13}C NMR (75 MHz, DMSO-d_6) δ 163.1, 158.1, 137.6, 136.2, 135.5, 129.1, 128.8, 128.1, 127.9, 127.2, 125.0, 123.9, 123.5, 122.0, 120.9, 120.6, 117.2, 113.6, 112.9, 69.5. HRMS (EI+) m/z ([M]+) calcd for $C_{22}H_{17}NO_3$ 343.12084; found 343.12070.

In Silico ADME Calculations

A set of physicochemical descriptors were computed using QikProp version 3.5 integrated into Schrödinger Molecular Modeling Suite (Schrödinger Release 2015-4, Schrödinger, LLC, New York). The QikProp descriptors are shown in Table 1. The 3D structures used in the calculation of QikProp descriptors were generated using Maestro (version 10.4,) and energy minimizations were carried out using Macromodel (version 9.9). Local minimum energy structures of each compound were used as input for ADME studies with QikProp.

Binding studies by surface plasmon resonance (SPR)

SPR experiments were performed at 25ºC with a Biacore X-100 apparatus (Biacore, GE) in HBS-EP (10 mM Hepes, 150 mM NaCl, 3 mM EDTA), with 2% de DMSO, 0.05% Tween 20 and 200 µM ATP when was required, at 25ºC. The protein AMPK was immobilized on a CM5 sensor chip (Biacore, GE) following the standard amine coupling method [32]. The carboxymethyl dextran surface of the flow cell 2 was activated with a 7-min injection of a 1:1 ratio of 0.4 M EDC and 0.1 M NHS. The protein was

coupled to the surface with a 300 s injection at several dilutions at 40 µg/ml in 10 mM sodium acetate, pH 5.0. The unreacted N-hydroxysuccinimide esters were quenched by a 7-min injection of 0.1 M ethanolamine-HCl (pH 8.0). The levels of immobilization were around 1000 RUs. Flow cell 1 treated as a flow cell 2 (amine coupling procedure) without protein was used as a reference. Prior to use, 10 mM stock solutions of compounds were diluted several times until 100 µM final concentration in the running buffer. Typically, a series of different compounds were injected onto the sensor chip with a flow rate of 30 µl/min for a period of 100 s followed by a dissociation period of 200 s. After the dissociation process, an extra wash treatment was made over the flow cells with a 50% DMSO solution. No regeneration was needed. For competition measurements between AMPK and different compounds, the concentrations used in the mixture were 100 µM for each one. Sensorgrams data were double-referenced and solvent corrected using the Biaevaluation X-100 software (Biacore, GE).

In vitro **Kinase Assay**

The AMPK (α1/β1/γ1) Kinase Enzyme System from Promega (Catalog number V1921) was used to screen AMPK inhibitors following the ADP-Glo™ Kinase Assay (Catalog number V9021). The assays were performed in 96-well plates (final volume 20 µl), the assay buffer contains 40 mM Tris, 7.5, 20 mM MgCl2, 0.1 mg/ml BSA and 50 µM DTT. 4 µl of activator was added to each well (final concentration of DMSO did not exceed 1%), followed by 8 µl of the enzyme (30 ng), after 5 min incubation at R/T, 8 µl of ATP (150 µM final concentration) and SAMStide (0.2 µg/µl) were added and incubated 60 min at room temperature, then ADP-Glo™ reagent (20 µL) was added allowing to incubate for 40 min at room temperature. Behind the incubation, the kinase detection agent (40 µL) was added and incubated for 30 min at room temperature.

Finally, the luminescence was recorded using an FLUO star Optima (BMG Labtechnologies GmbH, Offenburg, Germany) multimode reader. The activities were calculated based on the minimum activity, obtained in the absence of an activator.

Assessing AMPK activity in HEK293 cells

HEK293 cells were grown in DMEM media until they reached confluency. Then, cells were washed with KHR/Glu media (125 mM NaCl, 3 mM KCl, 1.5 mM CaCl$_2$, 0.5 mM MgSO$_4$, 0.5 mM KH$_2$PO$_4$, 2.5 mM NaHCO$_3$, 10 mM HEPES, pH: 7.4/ 25 mM Glucose) and maintained in this media supplemented or not with the appropriated concentration of different compounds for 1 h. Phenformin 5 mM and different doses of A-769662 (25 to 100 μM) were used as a positive control of AMPK activation. Then, cell lysis and protein extracts were obtained and analyzed as in Garcia-Haro et al., 2010 [33]. In brief, cell extracts (30 μg) were boiled in electrophoresis sample buffer and analyzed by SDS/PAGE and immunoblotting using appropriate antibodies: anti-phospho-AMPKα-Thr172 (#2535), anti-AMPKβ1 (#4182), anti-phospho-ACC-Ser79 (#3661), anti-ACC (#3662), anti-phospho-Raptor-Ser792 (#2083), anti-phospho-ULK1-Ser555 (#5869), anti-phospho-p38-Thr180/Tyr182 (#9211), and anti-phospho-JNK-Thr183/Tyr185 (#4668), were from Cell Signaling Technology (Hertfordshire, UK). Anti-αTubulin (T6199) was from Sigma. Secondary antibodies were from Santa Cruz Biotechnology (Santa Cruz, USA). Immunoblots were analyzed with the ECL+ reagent (GE Healthcare, Barcelona, Spain) and chemiluminescence was detected using a FUJIFILM LAS-3000 lite imager. Quantification of the bands was performed using the Image Studio lite v4.0 software.

Assessing the toxicity of selected compounds

HEK293 cells growing in DMEM were treated with different concentrations of the selected compounds for 24 hours. Then cell viability was determined using the cell-titer blue cell viability test from Promega, following the manufacturer's instructions.

C. elegans strains and maintenance

All strains were maintained at 20°C as described elsewhere.[34] N2 Bristol worms were used as standard wild type.[34] AM141 animals, with genotype *rmIs133[unc-54p::40Q::YFP]*[16], were obtained from the Caenorhabditis Genetics Center (CGC, Minneapolis, MN, USA). The strain RVM131: *vltEx131[mec-3p::112Q::TdTomato; myo-2p::GFP]* was previously generated in our laboratory.[10]

Drug assays on *C. elegans*

Synchronized L1 larvae were grown in 50 ml tubes with a final volume of 5 ml containing *E. coli* strain OP50 as a source of food (OD600=0.5), 50 µg/ml streptomycin, 12.5 µg/ml nystatin, 5 µg/ml cholesterol, and a specific amount of drug or vehicle, using M9 buffer as a solvent. IND1316 was used at a concentration of 50 µM. Worms were cultured at 20 °C under agitation until they reached the desired stage, for analysis.

Quantification of inclusion bodies in worms

The number of inclusion bodies was counted in approximately 60 L4 stage 40Q::YFP worms (AM141) by using a dissecting microscope equipped with fluorescence (Leica M165FC, Leica, Wetzlar, Germany). Each assay was repeated three times.

Touch assay on worms

The touch response of the worms was performed by gently passing an eyelash, mounted on a toothpick, on the posterior part of the 112Q::TdTomato worms (RVM131), as described elsewhere. [10,35] This assay was performed scoring the tail of each worm 10 touches for at least 30 animals, and the average of the response was plotted. Each assay was repeated three times.

Assessing the beneficial effect of IND1316 in zQ175 mice

The zQ175 mouse, provided by the CHDI Foundation, carries a normal murine Htt allele and a knock-in (KI) mutant *Htt*/*HTT* mouse/human hybrid allele containing approximately 190 CAG repeats. Heterozygous and wild type (WT) mice were generated by crossing heterozygous zQ175 mice in a C57BL/6J background. The genotype of the offspring was verified by PCR as in[10]. Only male mice were used in this study as a first approach to determine whether IND1316 treatment was able to ameliorate the HD phenotypes.

Three months old heterozygous and WT mice were treated with 36 mg/L of IND1316, administered ad libitum with the drinking water, for three months. This dose was the maximum solubility of the IND1316 in water. During this period, no differences in body weight or other health parameters were observed among treatment groups and control animals. A total of 16 heterozygous zQ175 and 16 wild type mice were used in this study, distributed as follows: 8 zQ175 and 8 WT received IND1316 treatment, and 8 zQ175 and 8 WT were left untreated.

A battery of behavioral tests at the beginning of the treatment (pre-treatment) and at the end (post-treatment) was performed. Experiments were performed with at least one- to two-day intervals between tests. The results were scored by a person blinded to genotype and treatment. We subjected all the animals to the following tests:

- Tail suspension test (TST): TST was developed as a rodent screening test for potential human antidepressant drugs [36]. To assess depressive-like behavior, mice were suspended by their tail for six minutes in an inescapable but moderately stressful situation. The lack of scape-oriented movements is considered immobility. The total immobility time was measured as an indicator of latency to defeat and despair against a stressful situation.

- Beam balance: Beam balance assesses fine motor coordination and balance in mice [37]. We analyzed the time taken to cross three beams of 30-, 12- and 5-mm width, 100 cm in length, and 50 cm in height above the floor. Training on day one and test on day three consisted of crossing three times each beam consecutively with an inter-trial interval of 10 minutes between beams.

Tissue collection and histopathological analysis

Animals were euthanized by cervical dislocation, brains were removed and immediately fixed in 4% paraformaldehyde (PAF) at 4ºC overnight, and embedded in paraffin for histological analysis. Sagittal brain slices from at least four independent mice per group were sectioned at 5 μm by microtome. Sections corresponding to Figure 107 of the Paxinus and Franklin's mouse brain atlas were dewaxed, rehydrated, and warmed at 95 °C for 20 min in 10 mM citrate buffer pH:6 for antigen retrieval. Sections were immersed in blocking buffer for 1 hour at room temperature and incubated O/N at 4°C with primary antibody diluted in the corresponding blocking buffer.

For immunohistochemistry, we used as blocking buffer 1% bovine serum albumin plus 5% fetal bovine serum in PBS, and as primary antibody anti-mHtt mEM48 (diluted 1/100; Merck Millipore ref. #MAB537). After three washes of 10 min in PBS, sections were incubated for 1 h at room temperature with the corresponding biotin-

conjugated anti-rabbit or anti-mouse secondary antibody (Jackson ImmunoResearch, West Grove, PA, USA) diluted in blocking buffer, washed three times with PBS for 5 min, and visualized with Avidin-Biotin Complex (ABC) (Vectastain Elite ABC Kit, Vector Laboratories, Burlingame, CA, USA) using diaminobenzidine as the chromogenic substrate for peroxidase (Peroxidase Substrate Kit DAB; Vector Laboratories, Burlingame, CA, USA). Sections were lightly counterstained with hematoxylin (Sigma, Madrid, Spain), dehydrated, and mounted in DPX (Merck, Germany). The immunostained tissue slides were imaged on a Leica Aperio Versa 200 Slide Scanner (Leica Biosystems). Sagittal brain slides were imaged at 40X magnification to a resolution of 0.136 μm/pixel.

For immunohistofluorescence, the blocking buffer of non-specific staining was 1% BSA, 10% FBS, 0.2% Triton X100, in PBS. The primary antibodies anti-glial fibrillary acidic protein (GFAP) (diluted 1/600; Sigma ref. #G3893), anti-ionized calcium-binding adaptor molecule 1 (IBA1) (diluted 1/200; Wako ref. #019-19741) were incubated overnight at 4 °C and washed 3 times during 10 min in PBS. Sections were incubated for one hour at room temperature with the appropriate secondary antibody diluted at 1/500 in blocking buffer without Triton X100, with the corresponding Alexa Fluor-conjugates [1:500, Life Technologies: goat anti-mouse IgG Alexa Fluor® 488 (#A11029) and goat anti-rabbit IgG Alexa Fluor® 594 (#A11012)) washed once with PBS, incubated with DAPI (Sigma, Madrid, Spain), washed twice with PBS, and mounted in AquaPolymount (Polysciences Inc., USA). Images were acquired in a Confocal Spectral Leica TCS SP8 microscope (Leica, Wetzlar, Germany) to measure GFAP intensity at 40 X magnification and single-plane automated tile scans were acquired using a DM6 B Thunder Imager 3D Tissue (Leica) at 20 X magnification

for Iba1 images processed with Thunder software (Leica) and mosaic-merged with 10% overlaps. The plane covered the whole brain hippocampus or a big part of the striatum.

In addition, we obtained mouse brain homogenates which were resuspended in lysis buffer [25 mM Tris-HCl, pH 7.4; 15 mM EDTA, 50 mM NaF, 15 mM $Na_2P_2O_7$, 0.6 M sucrose, 15 mM 2-mercaptoethanol and complete protease inhibitor cocktail (Roche, Barcelona, Spain)]. The homogenates were passed five times through a 25-gauge needle in a 2 ml syringe and centrifuged at 13,000xg for 10 min at 4ºC. Supernatants were collected and a total of 25 µg protein was subjected to SDS-PAGE and transferred onto a PVDF membrane. Membranes were blocked with 5% (w/v) nonfat milk in Tris-buffered saline (TBS-T: 50 mM Tris-HCl, 150 mM NaCl, pH 7.4) with 0.1% Tween-20 for 1 h at room temperature and incubated overnight at 4°C with the corresponding primary antibodies: anti-phospho-AMPKα-Thr172 (#2535), anti-AMPKβ1 (#4182), anti-phospho-ACC-Ser79 (#3661), anti-ACC (#3662) from Cell Signaling Technology (Hertfordshire, UK), and anti-αTubulin (T6199) from Sigma (Madrid, Spain). Then, membranes were probed with suitable secondary antibodies for 1 h at room temperature. Signals were obtained by chemiluminescence using an image reader Fuji-LAS-4000 (GE Healthcare, Barcelona, Spain) and Lumi-Light Western Blotting Substrate (Roche Applied Science, Barcelona, Spain). Experiments were performed on at least three individuals from each genotype. Quantification of the bands was performed using the Image Studio lite v4.0 software

Image acquisition and analysis

The acquired tiff images were processed with the ImageJ software (NIH, Bethesda, MD, USA) as follows. The area stained by mHtt antibody (huntingtin aggregates, brown) was calculated as a percent of the total analyzed area. We developed a macro for

automatic DAB stain detection and semiquantitative analysis. This macro included a background subtraction algorithm followed by color deconvolution calibrated to DAB and hematoxylin stains in individual stained slides. Two areas were extracted from the scanned images, the CA3 in the hippocampus and four different subareas in the striatum (values are the mean of these selected areas)

To quantify GFAP intensity, immunofluorescence images were acquired using a Leica TCS Sp8 laser-scanning confocal microscope with a × 40 objective. 10–12 z-axis stacks separated by 0.7 μm were taken per section, and 2D reconstruction was projected as maximum intensity using ImageJ software (NIH, Bethesda, MD, USA). For automated computer image analysis, we programmed tailored macros in ImageJ. Fluorescence images from Iba1 were first thresholded and % occupied area measured. The number of Iba1+ cells was manually counted for each acquired image.

All experiments were scored by a person blinded to genotype and treatment.

qRT-PCR analyses

The levels of expression of the pro-inflammatory markers TNFα and IL-1β were tested using SYBR green-based RT-qPCR. One ml of Tripure reagent (Roche Applied Science, Barcelona, Spain) was added to isolated striatums and tissue was disrupted by passing successively three times through a 25 gauge syringe. Total RNA was isolated according to the manufacturer's instructions. First strand cDNA was synthesized from 1 μg of total RNA using random hexamers and Expand reverse transcriptase (Roche Applied Science, Barcelona, Spain). cDNA was used as a template for real time PCR using PowerUp SYBR Green Master Mix (Applied Biosystems, Madrid, Spain), Protector RNase Inhibitor (Roche, Barcelona, Spain), MultiScribe Reverse Transcriptase (Applied Biosystems, Madrid, Spain) and specific

primers, according to the manufacturer's protocol. The gene-specific primers were synthesized by Sigma-Aldrich (Madrid, Spain). The primer sequences were: mTNFα-Forward ACGGCATGGATCTCAAAGAC; mTNFα-reverse GTGGGTGAGGAGCACGTAGT; mIL-1β-Forward CAGGCAGGCAGTATCACTCA; mIL-1β-reverse TGTCCTCATCCTGGAAGGTC. SYBR green-based RT-qPCR was performed under the following conditions: 50°C for 2 min and 95°C for 2 min, followed by 40 cycles of 95°C for 15 s, 60°C for 1 min, and 60°C to 95°C in increments of 0.5°C for 30 s to generate melting curves, on a Quant Studio 5 Real-Time PCR System (Applied Biosystems, Madrid, Spain). The data were processed using Quant Studio 5 software version 2.3 and expression values were calculated using the comparative Ct method. Each qPCR reaction was performed on three biological and three technical replicates from each sample. The GAPDH gene (GAPDH-Forward AATGTGTCCGTCGTGGATCTGA; GAPDH-Reverse GATGCCTGCTTCACCACCTTCT) was used as the endogenous reference control to normalize target gene expression. Values are expressed as $2^{\Delta\Delta Ct}$.

Data analysis

Statistical analysis was performed using GraphPad Prism 7 software. Quantitative data were represented as mean ± standard error mean (SEM). To assess the statistical significance (p-value) of the effects in multiple comparisons, data with a normal distribution were analyzed by two-way ANOVA followed by a Tukey's post hoc test.

AUTHOR INFORMATION

Corresponding Authors

*E-mail: acastro@iqm.csic.es Phone: +34915622900.

*E-mail: rafael_vazquez@iislafe.es Phone: +34961246678

*E-mail: sanz@ibv.csic.es Phone: +34963391779

ORCID

Ana Castro 0000-0001-7526-6717

Rafael Vázquez-Manrique 0000-0002-1594-0033

Pascual Sanz 0000-0002-2399-4103

Author Contributions

M.V., M.A.G-G, and A.S. contributed equally. A.C., P.S., and R.V-M. designed the project. M.V. and J.C. carried out the synthesis and analyzed the compounds. L.L. and C.P. performed the SPR analyses and the *in vitro* activation of AMPK experiments. E.P. performed ADME *in silico* studies. M.A.G-G carried out *in cell* experiments. A.S achieved *in vivo* experiments with mice. JB-Y performed the test on worms. A.C., P.S., and R.V-M. wrote the manuscript. All authors have read and agreed to the published version of the manuscript.

Notes

The authors declare no competing financial interest.

SUPPORTING INFORMATION: The supplementary material file contains supplementary Figures S1 and S2. Supplementary Figure S1 contains the whole information regarding Figure 4, in the main manuscript, for the sake of transparency. Figure S2 contains immunostaining of mHtt and inflammatory biomarkers, which did not yield positive results.

REFERENCES

(1) Saudou, F.; Humbert, S. The Biology of Huntingtin. *Neuron* **2016**, *89* (5), 910–926. https://doi.org/10.1016/j.neuron.2016.02.003.

(2) Leitman, J.; Ulrich Hartl, F.; Lederkremer, G. Z. Soluble Forms of PolyQ-Expanded Huntingtin Rather than Large Aggregates Cause Endoplasmic Reticulum Stress. *Nature Communications* **2013**, *4* (1), 1–10. https://doi.org/10.1038/ncomms3753.

(3) Bates, G. Huntingtin Aggregation and Toxicity in Huntington's Disease. *Lancet* **2003**, *361* (9369), 1642–1644. https://doi.org/10.1016/S0140-6736(03)13304-1.

(4) Ramamurthy, S.; Ronnett, G. V. Developing a Head for Energy Sensing: AMP-Activated Protein Kinase as a Multifunctional Metabolic Sensor in the Brain. *Journal of Physiology* **2006**, *574* (1), 85–93. https://doi.org/10.1113/jphysiol.2006.110122.

(5) Segatto, M.; Rosso, P.; Fioramonti, M.; Fracassi, A.; Marangoni, M.; Taglietti, V.; Siteni, S. AMPK in the Central Nervous System: Physiological Roles and Pathological Implications. *Research and Reports in Biology* **2016**, *7*, 1. https://doi.org/10.2147/rrb.s90858.

(6) Steinberg, G. R.; Carling, D. AMP-Activated Protein Kinase: The Current Landscape for Drug Development. *Nature Reviews Drug Discovery* **2019**, *18* (7), 527–551. https://doi.org/10.1038/s41573-019-0019-2.

(7) Salminen, A.; Kaarniranta, K.; Haapasalo, A.; Soininen, H.; Hiltunen, M. AMP-Activated Protein Kinase: A Potential Player in Alzheimer's Disease. *Journal of Neurochemistry* **2011**, *118* (4), 460–474. https://doi.org/10.1111/j.1471-4159.2011.07331.x.

(8)   Paudel, Y. N.; Angelopoulou, E.; Piperi, C.; Shaikh, M. F.; Othman, I. Emerging
        Neuroprotective Effect of Metformin in Parkinson's Disease: A Molecular
        Crosstalk. *Pharmacological Research* **2020**, *152*, 104593.
        https://doi.org/10.1016/j.phrs.2019.104593.

(9)   Ma, T. C.; Buescher, J. L.; Oatis, B.; Funk, J. A.; Nash, A. J.; Carrier, R. L.;
        Hoyt, K. R. Metformin Therapy in a Transgenic Mouse Model of Huntington's
        Disease. *Neuroscience Letters* **2007**, *411* (2), 98–103.
        https://doi.org/10.1016/j.neulet.2006.10.039.

(10)   Sanchis, A.; García-Gimeno, M. A.; Cañada-Martínez, A. J.; Sequedo, M. D.;
        Millán, J. M.; Sanz, P.; Vázquez-Manrique, R. P. Metformin Treatment Reduces
        Motor and Neuropsychiatric Phenotypes in the ZQ175 Mouse Model of
        Huntington Disease. *Experimental and Molecular Medicine* **2019**, *51* (6).
        https://doi.org/10.1038/s12276-019-0264-9.

(11)   Vázquez-Manrique, R. P.; Farina, F.; Cambon, K.; Dolores Sequedo, M.; Parker,
        A. J.; Millán, J. M.; Weiss, A.; Déglon, N.; Neri, C. AMPK Activation Protects
        from Neuronal Dysfunction and Vulnerability across Nematode, Cellular and
        Mouse Models of Huntington's Disease. *Human Molecular Genetics* **2015**, *25*
        (6), 1043–1058. https://doi.org/10.1093/hmg/ddv513.

(12)   Gómez-Escribano, A. P.; Bono-Yagüe, J.; García-Gimeno, M. A.; Sequedo, M.
        D.; Hervás, D.; Fornés-Ferrer, V.; Torres-Sánchez, S. C.; Millán, J. M.; Sanz, P.;
        Vázquez-Manrique, R. P. Synergistic Activation of AMPK Prevents from
        Polyglutamine-Induced Toxicity in Caenorhabditis Elegans. *Pharmacological
        Research* **2020**, *161*, 105105. https://doi.org/10.1016/j.phrs.2020.105105.

(13)   Hervás, D.; Fornés-Ferrer, V.; Gómez-Escribano, A. P.; Sequedo, M. D.; Peiró,
        C.; Millán, J. M.; Vázquez-Manrique, R. P. Metformin Intake Associates with

Better Cognitive Function in Patients with Huntington's Disease. *PLoS ONE* **2017**, *12* (6). https://doi.org/10.1371/journal.pone.0179283.

(14) WO2016042194A1 - Indole Derivatives for the Prevention and/or Treatment of Diabetes and Associated Metabolic Disorders, 2016.

(15) Arnoux, I.; Willam, M.; Griesche, N.; Krummeich, J.; Watari, H.; Offermann, N.; Weber, S.; Dey, P. N.; Chen, C.; Monteiro, O.; Buettner, S.; Meyer, K.; Bano, D.; Radyushkin, K.; Langston, R.; Lambert, J. J.; Wanker, E.; Methner, A.; Krauss, S.; Schweiger, S.; Stroh, A. Metformin Reverses Early Cortical Network Dysfunction and Behavior Changes in Huntington's Disease. *eLife* **2018**, *7*. https://doi.org/10.7554/eLife.38744.

(16) Morley, J. F.; Brignull, H. R.; Weyers, J. J.; Morimoto, R. I. The Threshold for Polyglutamine-Expansion Protein Aggregation and Cellular Toxicity Is Dynamic and Influenced by Aging in Caenorhabditis Elegans. *Proceedings of the National Academy of Sciences of the United States of America* **2002**, *99* (16), 10417–10422. https://doi.org/10.1073/pnas.152161099.

(17) Menalled, L. B.; Kudwa, A. E.; Miller, S.; Fitzpatrick, J.; Watson-Johnson, J.; Keating, N.; Ruiz, M.; Mushlin, R.; Alosio, W.; McConnell, K.; Connor, D.; Murphy, C.; Oakeshott, S.; Kwan, M.; Beltran, J.; Ghavami, A.; Brunner, D.; Park, L. C.; Ramboz, S.; Howland, D. Comprehensive Behavioral and Molecular Characterization of a New Knock-In Mouse Model of Huntington's Disease: ZQ175. *PLoS ONE* **2012**, *7* (12), e49838. https://doi.org/10.1371/journal.pone.0049838.

(18) Chermat, R.; Thierry, B.; Mico, J. A.; Steru, L.; Simon, P. Adaptation of the Tail Suspension Test to the Rat. *Journal de Pharmacologie* **1986**, *17* (3), 348–350.

(19)   Steru, L.; Chermat, R.; Thierry, B.; Mico, J. A.; Lenegre, A.; Steru, M.; Simon,

P.; Porsolt, R. D. The Automated Tail Suspension Test: A Computerized Device

Which Differentiates Psychotropic Drugs. *Progress in

Neuropsychopharmacology and Biological Psychiatry* **1987**, *11* (6), IN1-671.

https://doi.org/10.1016/0278-5846(87)90002-9.

(20)   Walter, C.; Clemens, L. E.; Müller, A. J.; Fallier-Becker, P.; Proikas-Cezanne, T.;

Riess, O.; Metzger, S.; Nguyen, H. P. Activation of AMPK-Induced Autophagy

Ameliorates Huntington Disease Pathology in Vitro. *Neuropharmacology* **2016**,

108, 24–38. https://doi.org/10.1016/j.neuropharm.2016.04.041.

(21)   Kung, P. J.; Tao, Y. C.; Hsu, H. C.; Chen, W. L.; Lin, T. H.; Janreddy, D.; Yao,

C. F.; Chang, K. H.; Lin, J. Y.; Su, M. T.; Wu, C. H.; Lee-Chen, G. J.; Hsieh-Li,

H. M. Indole and Synthetic Derivative Activate Chaperone Expression to Reduce

PolyQ Aggregation in SCA17 Neuronal Cell and Slice Culture Models. *Drug

Design, Development and Therapy* **2014**, *8*, 1929–1939.

https://doi.org/10.2147/DDDT.S67376.

(22)   Lin, C. H.; Wu, Y. R.; Kung, P. J.; Chen, W. L.; Lee, L. C.; Lin, T. H.; Chao, C.

Y.; Chen, C. M.; Chang, K. H.; Janreddy, D.; Lee-Chen, G. J.; Yao, C. F. The

Potential of Indole and a Synthetic Derivative for PolyQ Aggregation Reduction

by Enhancement of the Chaperone and Autophagy Systems. *ACS Chemical

Neuroscience* **2014**, *5* (10), 1063–1074. https://doi.org/10.1021/cn500075u.

(23)   Chen, C. M.; Chen, W. L.; Hung, C. T.; Lin, T. H.; Chao, C. Y.; Lin, C. H.; Wu,

Y. R.; Chang, K. H.; Yao, C. F.; Lee-Chen, G. J.; Su, M. T.; Hsieh-Li, H. M. The

Indole Compound NC009-1 Inhibits Aggregation and Promotes Neurite

Outgrowth through Enhancement of HSPB1 in SCA17 Cells and Ameliorates the

Behavioral Deficits in SCA17 Mice. *NeuroToxicology* **2018**, *67*, 259–269.

https://doi.org/10.1016/j.neuro.2018.06.009.

(24) Chen, K.; Qian, W.; Li, J.; Jiang, Z.; Cheng, L.; Yan, B.; Cao, J.; Sun, L.; Zhou,

C.; Lei, M.; Duan, W.; Ma, J.; Ma, Q.; Ma, Z. Loss of AMPK Activation

Promotes the Invasion and Metastasis of Pancreatic Cancer through an HSF1-

Dependent Pathway. *Molecular Oncology* **2017**, *11* (10), 1475–1492.

https://doi.org/10.1002/1878-0261.12116.

(25) Yuan, H.; Wang, T.; Niu, Y.; Liu, X.; Fu, L. AMP-Activated Protein Kinase-

Mediated Expression of Heat Shock Protein Beta 1 Enhanced Insulin Sensitivity

in the Skeletal Muscle. *FEBS Letters* **2017**, *591* (1), 97–108.

https://doi.org/10.1002/1873-3468.12516.

(26) Kuemmerle S, Gutekunst CA, Klein AM, Li XJ, Li SH, Beal MF, Hersch SM, F.

R. Huntington Aggregates May Not Predict Neuronal Death in Huntington's

Disease. *Ann Neurol* **1999**, *46* (6), 842–849.

(27) Miller, T. W.; Shirley, T. L.; Wolfgang, W. J.; Kang, X.; Messer, A. DNA

Vaccination against Mutant Huntingtin Ameliorates the HDR6/2 Diabetic

Phenotype. *Molecular Therapy* **2003**, *7* (5), 572–579.

https://doi.org/10.1016/S1525-0016(03)00063-7.

(28) Weiss, K. R.; Kimura, Y.; Lee, W. C. M.; Littleton, J. T. Huntingtin Aggregation

Kinetics and Their Pathological Role in a Drosophila Huntington's Disease

Model. *Genetics* **2012**, *190* (2), 581–600.

https://doi.org/10.1534/genetics.111.133710.

(29) Arawaka, S.; Fukushima, S.; Sato, H.; Sasaki, A.; Koga, K.; Koyama, S.; Kato, T.

Zonisamide Attenuates α-Synuclein Neurotoxicity by an Aggregation-

Independent Mechanism in a Rat Model of Familial Parkinson's Disease. *PLoS ONE* **2014**, *9* (2). https://doi.org/10.1371/journal.pone.0089076.

(30) Carty, N.; Berson, N.; Tillack, K.; Thiede, C.; Scholz, D.; Kottig, K.; Sedaghat, Y.; Gabrysiak, C.; Yohrling, G.; von der Kammer, H.; Ebneth, A.; Mack, V.; Munoz-Sanjuan, I.; Kwak, S. Characterization of HTT Inclusion Size, Location, and Timing in the ZQ175 Mouse Model of Huntington's Disease: An in Vivo High-Content Imaging Study. *PLoS One* **2015**, *10* (4), e0123527. https://doi.org/10.1371/journal.pone.0123527.

(31) Reindl, W.; Baldo, B.; Schulz, J.; Janack, I.; Lindner, I.; Kleinschmidt, M.; Sedaghat, Y.; Thiede, C.; Tillack, K.; Schmidt, C.; Cardaun, I.; Schwagarus, T.; Herrmann, F.; Hotze, M.; Osborne, G. F.; Herrmann, S.; Weiss, A.; Zerbinatti, C.; Bates, G. P.; Bard, J.; Munoz-Sanjuan, I.; Macdonald, D. Meso Scale Discovery-Based Assays for the Detection of Aggregated Huntingtin. *PLoS One* **2019**, *14* (3), e0213521. https://doi.org/10.1371/journal.pone.0213521.

(32) Johnsson, B.; Löfås, S.; Lindquist, G. Immobilization of Proteins to a Carboxymethyldextran-Modified Gold Surface for Biospecific Interaction Analysis in Surface Plasmon Resonance Sensors. *Analytical Biochemistry* **1991**, *198* (2), 268–277. https://doi.org/10.1016/0003-2697(91)90424-R.

(33) Garcia-Haro, L.; Garcia-Gimeno, M. A.; Neumann, D.; Beullens, M.; Bollen, M.; Sanz, P. The PP1-R6 Protein Phosphatase Holoenzyme Is Involved in the Glucose-Induced Dephosphorylation and Inactivation of AMP-Activated Protein Kinase, a Key Regulator of Insulin Secretion, in MIN6 Beta Cells. *The FASEB journal : official publication of the Federation of American Societies for Experimental Biology* **2010**, *24* (12), 5080–5091. https://doi.org/10.1096/fj.10-166306.

(34)   Brenner, S. The Genetics of Caenorhabditis Elegans. *Genetics* **1974**, *77* (1), 71–94.

(35)   Parker, J. A.; Connolly, J. B.; Wellington, C.; Hayden, M.; Dausset, J.; Neri, C. Expanded Polyglutamines in Caenorhabditis Elegans Cause Axonal Abnormalities and Severe Dysfunction of PLM Mechanosensory Neurons without Cell Death. *Proceedings of the National Academy of Sciences of the United States of America* **2001**, *98* (23), 13318–13323. https://doi.org/10.1073/pnas.231476398.

(36)   Can, A.; Dao, D. T.; Terrillion, C. E.; Piantadosi, S. C.; Bhat, S.; Gould, T. D. The Tail Suspension Test. *Journal of Visualized Experiments* **2011**, No. 58, 3769. https://doi.org/10.3791/3769.

(37)   Brooks, S. P.; Dunnett, S. B. Tests to Assess Motor Phenotype in Mice: A User's Guide. *Nature Reviews Neuroscience*. Nature Publishing Group July 10, 2009, pp 519–529. https://doi.org/10.1038/nrn2652.

SUPPLEMENTARY MATERIAL

Supplementary Figures

Supplementary Figure S1. Complete figure corresponding to Figure 4. In that Figure, the lane corresponding to the metformin treatment was omitted since the product did not work under our conditions.

DAPI GFAP Iba1
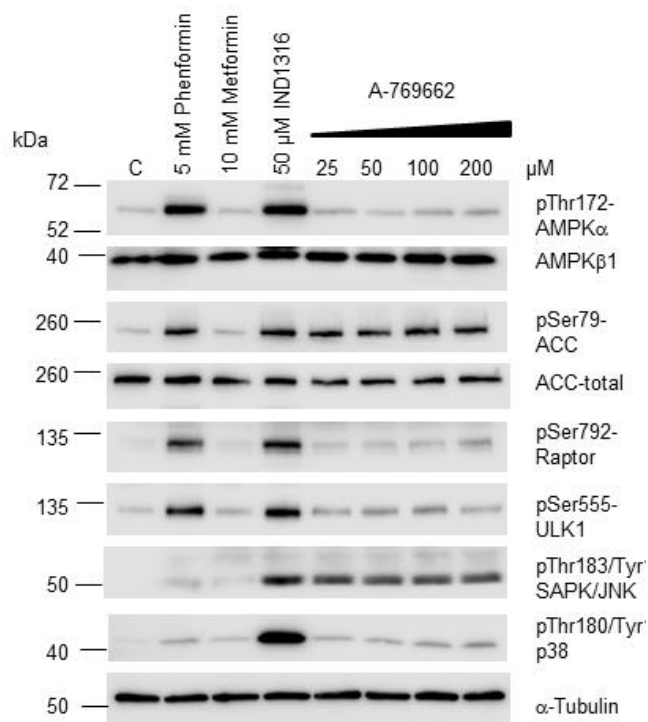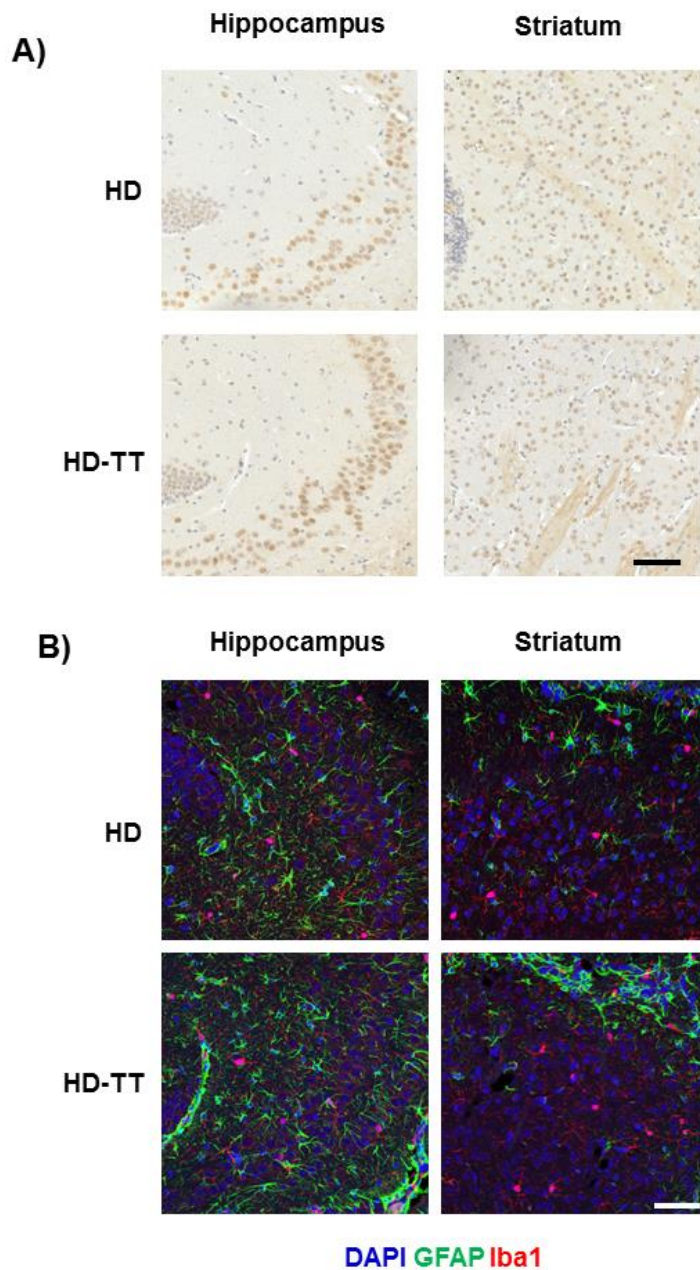
Supplementary Figure S2: IND1316 does not affect the number of mHtt aggregates or the presence of neuroinflammatory markers in zQ175 mice. A) Brain samples from zQ175 treated and untreated mice were analyzed by immunohistochemistry using anti-mHtt antibodies. A representative image of the mHtt aggregates in two areas of the brain, hippocampus, and striatum is shown. No statistically significant differences were found (n: 5). B) Immunofluorescence analysis with anti-GFAP (green signal) and with

anti-Iba1 (red signal) showed no differences in the intensity of these two neuroinflammatory markers in samples from zQ175 treated and untreated animals (n: 4). Representative images of these analyses are shown. HD: untreated zQ175 mice; HD-TT: treated zQ175 mice. Bars, 50 μm.